Determination of Biomolecular Oligomerization in the Live Cell Plasma Membrane via Single-Molecule Brightness and Co-localization Analysis

Clara Bodner and Mario Brameshuber

Contents

Abstract Oligomerization of biomolecules on the plasma membrane drives vital cellular functions. Despite the importance of detecting and characterizing these molecular interactions, there is an apparent lack of proper techniques capable of unraveling the exact composition of multimolecular complexes directly on the (live) cell membrane, particularly when present at high surface densities. In this chapter, commonly applied single-molecule fluorescence microscopy approaches are reviewed in terms of their suitability for detecting molecular aggregates down to

C. Bodner and M. Brameshuber (✉)
TU Wien, Institute of Applied Physics, Biophysics, Vienna, Austria
e-mail: bodner@iap.tuwien.ac.at; brameshuber@iap.tuwien.ac.at

R. Šachl, M. Amaro (eds.), *Fluorescence Spectroscopy and Microscopy in Biology*,
Springer Ser Fluoresc (2023) 20: 277–304, https://doi.org/10.1007/4243_2022_25,
Published online: 4 August 2022

the smallest biologically relevant unit: a molecular dimer. Amongst these techniques, Thinning Out Clusters while Conserving Stoichiometry of Labeling (TOCCSL) – a modality based on single-molecule brightness and co-localization analysis – is discussed in detail. The chapter lists basic principles of TOCCSL, its implementation on single-molecule fluorescence microscopes, analysis of brightness and co-localization-based microscopy data, and guidelines on how to choose parameters and labels to determine the number of labeled subunits within a multimolecular assembly. At the end, a tabular list of TOCCSL applications conducted so far is provided.

Keywords Brightness analysis · Co-localization analysis · Multimolecular complexes · Plasma membrane structure · Single-molecule microscopy · Thinning out clusters while conserving stoichiometry of labeling (TOCCSL)

1 Biomolecular Interactions on the Plasma Membrane

Life is all about interactions: from a simple handshake or a meaningful eye contact between humans, down to complex interactions between single cells and organelles, further down to the interactions of individual (bio)molecules, and even further down to nucleonic interactions between the smallest building blocks of life. On the intermediate length scale, molecular interactions drive the specific assembly of biomolecules into multimolecular structures. One of the major matrices for hosting these biomolecular interactions is the plasma membrane, as it represents the interface of a biological cell and the extracellular environment. Interactions occur between molecules of the same kind (homo-interactions), or between different species (hetero-interactions) and result in different aggregation states, ranging from the simplest form – a homo-dimer – to large multimolecular structures hosting a diverse set of biomolecules (see Fig. 1 for examples of biomolecular interactions on the plasma membrane of mammalian cells).

Some interactions between molecules are extremely stable and occur already before molecules reach the plasma membrane, as it is required for the correct function of various protein complexes. For example, only the complete assembly of the octameric T cell receptor CD3 complex (TCR/CD3) results in its sorting to the plasma membrane and facilitates highly sensitive and specific antigen-recognition during immune cell signaling [1].

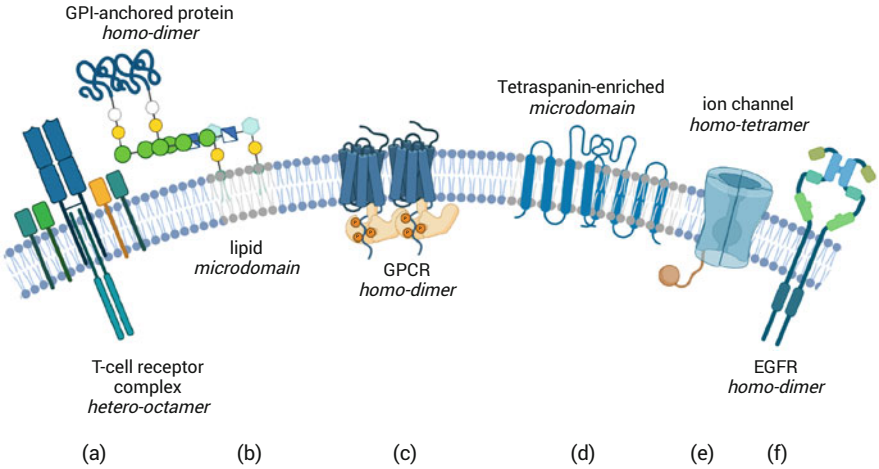

Fig. 1 Examples of biomolecular interactions and assemblies. From left to right: (**a**) The TCR/CD3 complex consists of three hetero-dimers with extracellular domains (αβ, δε, and γε subunits) and the ζ-chain homo-dimer with intracellular immunoreceptor tyrosine-based activation motifs (ITAMs). The αβ hetero-dimer is responsible for binding the antigen presented via MHC class I or II proteins on antigen-presenting cells (APC). (**b**) A class of proteins anchored via a GPI moiety is targeted to the extracellular side of the plasma membrane and the homo-association of such proteins is ascribed important cellular signaling functions. The lipid anchor is also responsible for allocating these proteins to lipid microdomains. (**c**) The minimal functional form of GPCR is represented by a homo- or hetero-dimer. (**d**) Another type of microdomain is reported to be enriched in proteins containing four transmembrane domains – so-called tetraspanins. Via homo-associations, these tetraspanins can form large networks on the cell membrane. (**e**) Most ion channels are homo- or hetero-tetramers and responsible for the controlled conductance of various ions through the plasma membrane. (**f**) The epidermal growth factor receptor (EGFR) is a transmembrane protein and described to form homo-dimers responsible for signaling. The receptor plays an important role in many cancer types, where mutations influence EGFR expression or activity. Created with BioRender.com

In this chapter, TCR/CD3 will serve as a model system representing a multimolecular complex. The α-β hetero-dimer, which is responsible for antigen binding, the δ-ε and γ-ε hetero-dimer, as well as the ζ-ζ homo-dimer containing intracellular domains transmitting the signal of antigen recognition (see Fig. 2) represent the eight subunits. Different techniques will be discussed in terms of their capability to detect the number of ε- and β-subunits directly at their place of action: the plasma membrane of a living T cell.

Stable homo- or hetero-association of four subunits represents the functional state of many ion channels, for example, the voltage-gated potassium channels [3, 4], with the composition being critical for correct function.

Interactions might also occur directly on the plasma membrane leading – in the simplest form – to a transient homo-dimer. For guanine nucleotide-binding (G-)

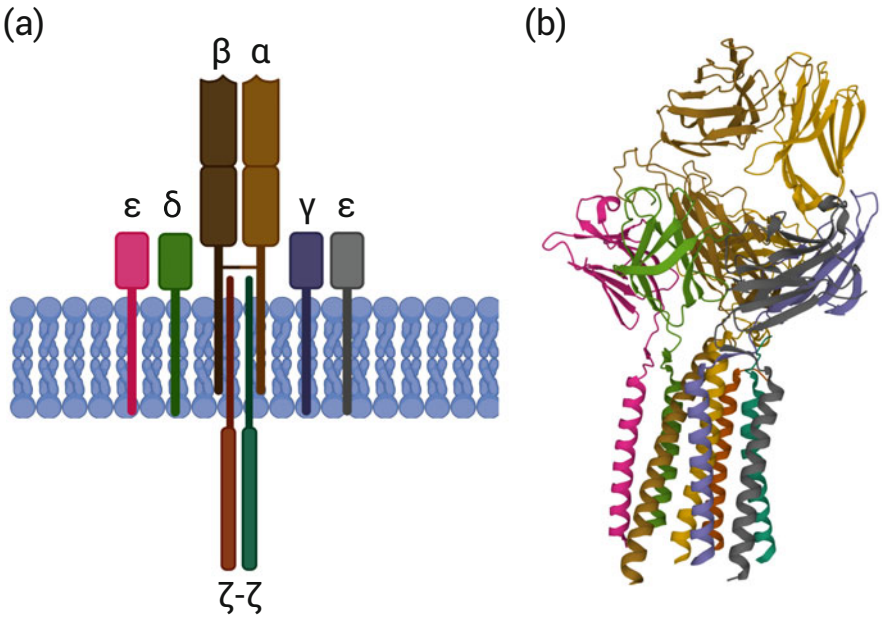

Fig. 2 Structure of the αβTCR/CD3 complex. (**a**) Sketch of the subunit assembly showing the α-β, δ-e, and γ-ε hetero-dimer, as well as the intracellular ζ-ζ homo-dimer. (**b**) Extracellular domains and transmembrane helices of the human TCR/CD3 complex as determined by cryo-electron microscopy [2]. Color coding same as in (**a**). PDB ID 6JXR. Created with BioRender.com

protein-coupled receptors (GPCRs) – a major target for pharmaceutical drugs – such a dimer was found to be the minimal functional structure, however, with considerable variations as the existence of hetero-dimers and the formation of larger complexes was also described to be required for signaling [5]. Another family of proteins, receptor tyrosine kinases, was described to form homo- and hetero-dimeric structures, as well as much larger complexes, which in turn activate the intracellular kinase domains to initiate signaling [6].

Much more transient interactions on the plasma membrane with lifetimes below 200 ms have been described for glycosyl-phosphatidylinositol (GPI) anchored proteins, including CD59, Thy1 and DAF [7, 8] and have been ascribed essential cellular functions. Larger biomolecular assemblies like tetraspanin-enriched microdomains [9] or lipid microdomains (“rafts”) [10] were found to contain hundreds of different constituents and play important roles for the function of adhesion receptors and the compartmentalization of enzymatic activities, and are discussed as platforms for signaling, exocytosis, and endocytosis, respectively.

While the importance of these biomolecular assemblies for cellular functions is indisputable, there is an apparent lack of proper technologies capable of unraveling the exact composition of multimolecular complexes directly on the (live) cell membrane. Why is it so much harder to look at the interaction of two molecules than to take a picture of two close-by humans shaking hands? The main reason is,

that human interactions happen on the same length (and time) scale for both, the observer and the observed, while the scales differ up to 9 orders of magnitude between single molecules and a human observer. One commonly used approach to tackle this discrepancy is to modify molecules of interest by binding a fluorescent molecule of similar size and use ultrasensitive fluorescence microscopy to directly visualize single molecules and multimolecular complexes.

2 Detecting Biomolecular Assemblies Directly on the Plasma Membrane

Equipped with powerful light sources and a sensitive detection camera, fluorescence microscopes are nowadays routinely used to observe single fluorescent molecules and should in principle be capable of detecting the smallest unit of a biomolecular assembly – a molecular dimer.

For the example of the TCR/CD3 complex, which contains two ε-subunits (the two outer subunits shown in Fig. 2), ideally all ε-subunits on the surface of a T cell can be fluorescently labeled. With an average expression level of 10^4 TCRs per cell and a T cell diameter of ~5 μm, the TCR density yields around 130 TCR complexes located within 1 μm^2 of the cell membrane. The average distance between TCRs is $1/\sqrt{130\ \mu m^{-2}} = 90$ nm, which is far below the optical resolution limit of a light microscope defined by the width of the point spread function (PSF) of the optical system. The typical size of the PSF, given by $0.61\frac{\lambda}{NA}$, with λ being the emission wavelength and NA the numerical aperture of the used objective, yields ~200 nm for visible light and the use of a high NA-objective. Avoiding overlapping PSFs hence limits molecule densities to values below one molecule per μm^2 for the unambiguous detection of individual fluorophores. Thus, the density of the TCR is about 1,000-fold too high for the direct imaging of ε-subunit dimers. The experimenter would observe a homogeneous fluorescence signal throughout the plasma membrane of non-stimulated T cells. Which strategies applicable in single-molecule fluorescence microscopy would now allow for the detection of these TCR ε-dimers at high surface densities?

2.1 How About Decreasing the Label Density?

Decreasing the label density on the cell membrane by a factor of ~1,000 for the observation of individual diffraction-limited signals can be realized by photobleaching [11], for example, by increasing the laser power and illumination time, by reducing the label concentration [12], or by photoactivating a subset of molecules [13]. Importantly, the label density will be reduced stochastically using these approaches, i.e., most TCR ε-dimers will become invisible due to the loss or

lack of detectable labels or become apparent monomers with only one fluorescent label per ε-dimer visible. Only a minor fraction of detectable ε-dimers will remain with both ε-subunits carrying fluorescent labels. Hence, the likelihood for observing an ε-dimer will decrease substantially. Assuming 100% ($p_{\text{coloc}} = 1$) ε-dimers and a reduction of the surface density by a factor of 1,000 ($p_{\text{label}} = 10^{-3}$), an experiment would yield a probability for co-localization of the two ε-subunits of

$$p = \frac{p_{\text{label}} p_{\text{coloc}}}{1 + p_{\text{coloc}}(1 - p_{\text{label}})} \approx \frac{p_{\text{label}}}{2} = 5 \times 10^{-4}.$$

In words, only 5 out of 10,000 visible ε-subunits would be paired with another visible ε-subunit within the same TCR/CD3 complex. This small fraction cannot be straightforward detected with standard single-molecule fluorescence microscopy techniques. Detection of such low fractions demands for highly quantitative microscopy tools and enormous amounts of data to gain sufficient statistics for a reliable proof of the existence of a few ε-dimers.

2.2 *Would One of the Single-Molecule Localization Microscopy (SMLM) Modalities Work for Detecting Molecular Dimers?*

Photoactivated localization microscopy (PALM) [14, 15] and (direct) stochastic optical reconstruction microscopy ((d) STORM) [16, 17] are based on the fact, that a single, separated molecule can be localized with a much higher precision – even down to the sub-nanometer level [18] – than the diffraction limit of the optical system. These so-called SMLM or superresolution microscopy approaches (for a recent review see [19]) are nowadays routinely used to resolve cellular structures well below the diffraction limit (see Chap. 10 "Quantitative Photoactivated Localization Microscopy of Membrane Receptor Oligomers" for details on SMLM techniques). In contrast to the aforementioned strategies for decreasing the label density per image, in SMLM all molecules of interest are fluorescently labeled but are not visible at the same time in the detection channel. Only a few of these fluorescent molecules are stochastically activated by switching them into a bright or red-shifted fluorescent state and can be detected as diffraction-limited signals. Detected molecules are deactivated by either switching them back to a dark or blue-shifted state, or by terminal photobleaching. Tens of thousands of these activation-detection-deactivation cycles increase the probability of detecting a high fraction of – for the TCR as an example – ε-subunits. Localizing each individual signal in all recorded frames finally yields a reconstructed image with a theoretical resolution in the order of the localization precision. Optimizing photon yield and background noise could result in a superresolution image with a resolution one order of magnitude lower than the 90 nm average distance of TCR molecules. An ideal quantitative superresolution

experiment would hence allow to detect individual ε-dimers. What was neglected so far?

1. Diffusional motion of the TCR/CD3 complex on the cell membrane heavily influences the reconstructed image. Due to the stochastic activation process, the individual ε-subunits of one TCR complex are imaged at different experimental time points – and hence different positions on the cell membrane – and the assignment of both subunits to the same complex is impossible. With a diffusion coefficient of ~0.04 $\mu m^2/s$ [20], the total recording time of the superresolution image would need to be shorter than 0.6 ms to virtually freeze the motion of the structure at the resolution of 10 nm and to observe ε-dimers. However, the photon budget needed for 10 nm resolution as well as technical limitations result in typical recording times of several seconds.
2. Chemical fixation is often performed to "freeze" the movement and to record a snapshot of the oligomerization state of certain proteins. This is also possible for the TCR/CD3 complex, and superresolution images can be analyzed in terms of clustering and oligomerization [21]. However, the repeated detection and subsequent localization of one and the same molecule within the localization precision limit, as well as the presence of a dark fraction of fluorophores renders quantitative superresolution imaging down to small nanoclusters or even individual dimers extremely challenging (see [22] for a review on the difficulties in detecting nanocluster). While there are several algorithms available to account for very well-defined blinking patterns of fluorescent molecules, the presence of only a few outliers can change the interpretation of results completely [21, 23]. Even with perfectly behaving fluorophores, i.e., clearly defined blinking patterns or no blinking at all, residual motion of proteins despite fixation needs to be considered [24]. One possible solution to overcome residual motion and potential chemical fixation artifacts is to conduct superresolution microscopy experiments at cryogenic temperatures [25–27]. Current technical developments and first applications look promising for using cryoSMLM for the routine detection and characterization of biomolecular assemblies at the plasma membrane in the near future.

2.3 How about Using Stimulated Emission Depletion (STED) Imaging?

STED microscopy [28, 29] (for reviews see, e.g., [30–32] has proved to be a meaningful approach to significantly improve the resolution of fluorescence images without the necessity of utilizing the stochastic blinking of fluorophores. Instead, fluorescence in the periphery of a focused excitation beam is efficiently quenched by a depletion laser (see Chap. 7 "STED and RESOLFT Fluorescent Nanoscopy" for more details on STED microscopy). Nowadays, a spatial resolution of ~60 nm can be routinely achieved in STED microscopy which, keeping the TCR as an example, enables the direct detection of individual TCR/CD3 complexes labeled via their

ε-subunits on chemically fixed T cells [21]. Despite STED being a scanning technique, in which the excitation and depletion lasers are concomitantly moved over the sample, joining scan lines are recorded fast enough for neglecting residual motion of molecules on fixed cells. Frame rates achieved nowadays even allow STED imaging on live cells and the detection of biomolecular clustering on length scales larger than the resolution limit of STED microscopy. Determination of the composition of protein oligomers using STED by directly visualizing all labeled constituents is in most cases prevented by the limited resolution. However, unambiguously counting the exact number of dye molecules per molecular complex is possible via analysis of coinciding photon arrival times (photon antibunching, PA) [33–35] and enables the direct detection of ε-dimers within the TCR/CD3 complex in fluorescence correlation spectroscopy (FCS) experiments [20]. Combining STED imaging with PA seems ideal for the stoichiometric analysis of protein complexes at high surface densities, but requires costly and specialized equipment [36]. A recently introduced STED-related approach based on minimal photon fluxes (MINFLUX) might be an alternative method for the direct observation of molecular complexes at nanometer resolution [37, 38].

2.4 Thinning Out Clusters While Conserving Stoichiometry of Labeling (TOCCSL)

In contrast to the above-mentioned strategies i–iii, an easy-to-implement single-molecule fluorescence modality termed TOCCSL [39, 40] allows to determine the number of labeled subunits within a multimolecular assembly – also at high surface densities on the membrane of live cells. The approach is based on a FRAP (fluorescence recovery after photobleaching [41, 42]) protocol, with the main difference, that individual oligomers are detected at the onset of the very recovery process when the density of molecules is low enough to resolve single entities. In the following, the TOCCSL principle, experimental strategies, and considerations, as well as on overview of TOCCSL applications are discussed.

3 The TOCCSL Concept

3.1 Principle

In the plasma membrane, the physiological surface density of biomolecules is usually too high to resolve individual fluorescently labeled protein clusters, as their size and the average distance between two adjacent molecular aggregates are smaller than the resolution limit of light microscopy. The single-molecule fluorescence microscopy method TOCCSL [40, 43] is used to study the stoichiometry of cell surface proteins (or lipids) in life cells and model systems at physiologically high densities. The principle of TOCCSL is shown in Fig. 3.

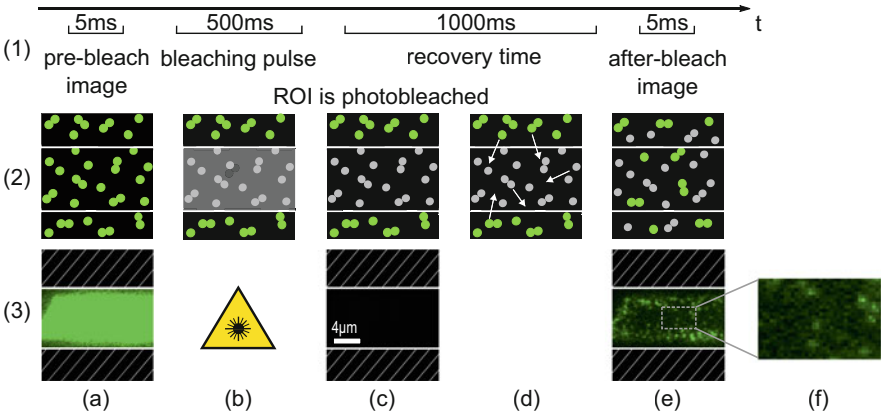

Fig. 3 A typical TOCCSL imaging protocol. (1) Illumination timing scheme. (2) Schematic illustration: (**a**) A control image (pre-bleach image) is taken at low laser intensity, which is used to determine the molecule density on the cell surface. (**b**) A short high-intensity laser pulse is applied which causes the region of interest (ROI), defined by an aperture, to be irreversibly photobleached. (**c**) A few milliseconds after the bleaching pulse, another control image can be taken to ensure that all molecules within the field of view are completely photobleached. (**d**) At the onset of the recovery process fluorescent molecules from the shielded area diffuse into the photobleached region and can be imaged as diffraction-limited spots (**e**). (**f**) Zoomed region from (**e**). (3) Example of a TOCCSL experiment. CHO cells expressing GPI-anchored SNAP were labeled with Alexa Fluor 488. Note that the contrast is identical for pre-bleach image, control image, and after-bleach image

One can consider the TCR/CD3 protein complex labeled via the two ε-subunits as an example (see Fig. 3. Note, that a more general example of a molecule existing as monomer and homo-dimer is sketched). Using TOCCSL, the surface density of active fluorophores in a small region of the cellular plasma membrane is transiently depleted by applying a high-intensity laser pulse (several kW/cm^2) to a defined area of the cell surface using an aperture. By doing so, all fluorophores within the illuminated region are irreversibly photobleached, while the stoichiometric composition of TCR/CD3 complexes remains unaltered: both labels of ε-subunits are either photobleached or are intact because they were not exposed to laser light. Due to Brownian motion, fluorescently labeled TCR/CD3 molecules from outside the aperture-defined area of the biomembrane can diffuse into the photobleached region during a short recovery time (several hundred ms up to several seconds). Using ultrasensitive fluorescence microscopy, single protein clusters can be imaged as diffraction-limited spots at the onset of this recovery process.

3.2 Imaging Protocol

Figure 3 illustrates a typical TOCCSL experiment with the timing protocol for sample illumination shown on the top. First, an image at low laser intensity with

illumination time t_{ill} is taken in total internal reflection (TIR) configuration to report the initial situation of high surface density. A high-intensity laser pulse is then applied in TIR or non-TIR configuration for a bleaching time t_{bleach}. During a short recovery time t_{rec}, molecules from the shielded area diffuse into the photobleached region, where they are imaged directly after t_{rec} in TIR configuration. Both laser intensity and t_{bleach} are chosen such, that all active fluorophores within the aperture-defined area are fully photobleached as fast as possible, to avoid incompletely or partially bleached protein clusters, where one or more protein subunits remain fluorescent. For the TCR/CD3 complex partial bleaching of ε-dimers would yield a wrong composition of some TCR/CD3 complexes containing only one apparent-fluorescent ε-subunit. t_{rec} is chosen in a way that the surface density of single fluorescently labeled protein clusters in the inner region of the photobleached area remains low enough, such that single molecules can be resolved. The choice of t_{rec} and t_{ill} depends on the diffusion coefficient of the observed biomolecule and for t_{rec} it also depends on the surface density as well as the chosen aperture-size (for more details, see Sect. 5).

3.3 Brightness Analysis

Generally, the image of a point-like source of light is represented by its PSF, which exhibits an Airy disc in the center and decreasing intensities towards the radial direction. For this reason, a two-dimensional Gaussian function represents a good approximation for the PSF of a single point-like emitter, e.g., a single dye molecule or a fluorescent protein. The location of a fluorescent molecule can be determined, e.g., by identifying the center of the Gaussian fit. While the exact position and its precision are important parameters for SMLM, the integral of the Gaussian is used for the analysis of TOCCSL images and yields the overall number of emitted photons during t_{ill}, i.e., the brightness of the molecular complex. It is also possible to calculate the brightness directly from raw images via the sum of individual pixel values at the position of diffraction-limited signals corrected by the local background. Besides providing a more realistic photon estimation, this is particularly useful for long illumination times, where diffusion of molecular complexes yields asymmetric PSFs [44]. Note that often pixel values are not displayed in units of photons but rather counts and hence need to be corrected by considering the (electron multiplication) gain and electrons-per-count conversion factor.

In TOCCSL, the statistical distribution of fluorescently labeled subunits per protein cluster is determined via brightness analysis of the diffraction-limited single-molecule signals, which are imaged according to their PSF [40]. The photon emission of a single fluorescent molecule is stochastic. Thus, the number of photons F detected from a single fluorescent emitter cannot be determined precisely but is characterized by the probability density function (pdf) $\rho_1(F)$. $\rho_1(F)dF$ is the probability that the number of detected photons determined by a brightness measurement of a single-molecule signal lies within the interval $[F, F + dF]$. To determine the pdf

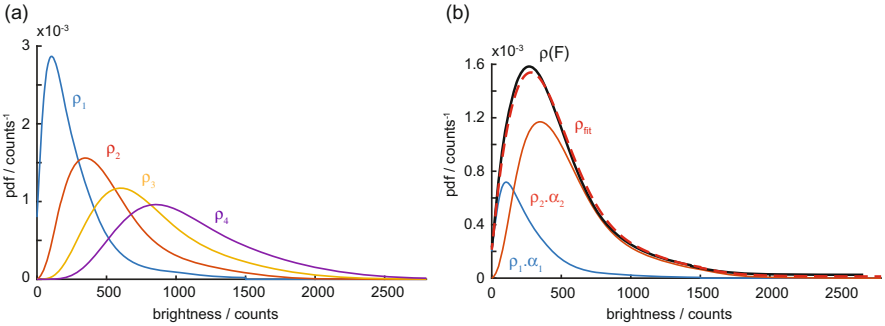

Fig. 4 Brightness-based analysis of a TOCCSL experiment. (**a**) By measuring the brightness distribution of single molecules, ρ_1, the corresponding distributions of 2, 3, or 4 molecules can be calculated via convolution integrals assuming independent emitters. Note that all distributions are normalized to 1. (**b**) The normalized pdf of measured fluorescence signals of protein clusters, $\rho(F)$, is fitted by a linear combination of various N-mer contributions, ρ_{fit}. Since all distributions are normalized, the area under contributing pdfs directly yields the fraction of N-mers. For the example shown, $\rho(F)$ is decomposed into a fraction of 25% monomers (α_1) and 75% dimers (α_2). Shown data is based on a simulation of 500 and 1,000 log-normal distributed brightness values [45] for ρ_1 and $\rho(F)$, respectively

of a single emitter, ρ_1, the fluorescence brightness values of individual fluorophores can be acquired experimentally by stepwise decreasing the emitted fluorescence of protein clusters through photobleaching of the sample, until most fluorophores are irreversibly photobleached and a few single-molecule signals exhibit their lowest brightness value (monomeric signal). Single molecules can also be tracked throughout the photobleaching process to ensure that the lowest brightness level within one photobleaching trace is used to determine ρ_1. If possible, under-labeling of molecular subunits might also yield the brightness distribution of single-molecule signals. In the case of the TCR/CD3 complex, decreasing the label density by a factor of ~1,000 will yield a good approximation of the ε-subunit monomer distribution with a neglectable fraction of ε-dimers contributing to this distribution (see Sect. 2.1).

Assuming higher order oligomers of order N, the brightness distribution of N co-localized independent emitters, $\rho_N(F)$, can be determined recursively from the single-dye brightness pdf ρ_1 as a series of convolution integrals $\rho_N(F) = \int \rho_1(F')\rho_{N-1}(F - F')dF'$ (see Fig. 4a).

When recording the fluorescence of a mixed monomer and higher order N-mer population, the resulting brightness distribution, $\rho(F)$, is based on a linear combination of the previously determined individual pdfs of each N-mer population, $\rho_N(F)$, weighted with the fraction of the respective oligomer of degree N, α_N:

$$\rho(F) = \sum_{N=1}^{N_{\max}} \alpha_N \times \rho_N(F) \tag{1}$$

with

$$\sum_{N=1}^{N_{\max}} \alpha_N = 1 \tag{2}$$

The pdf of the fluorescence signal of protein clusters, $\rho(F)$, is determined from a TOCCSL experiment. By non-linear least squares fitting of $\rho(F)$ with Eq. (1) the relative N-mer fractions α_N can be calculated (see Fig. 4b for an example).

For determining the stoichiometry of the TCR/CD3 complex, the β-subunit was fluorescently labeled and ρ_N was determined in a TOCCSL experiment [20]. ρ_1 was obtained from the same experiment after prolonged and repeated photobleaching or, alternatively, from recording T cells with 150-fold substoichiometric TCR labeling. Analysis yielded a small fraction (3% ± 4%) of potential dimeric TCRβ dimers. The aforementioned labeling of the ε-subunits served as a positive-control: using TOCCSL, 74% ± 4% of TCR/CD3 complexes returning to the photobleached area contained two ε-subunits. Taken together, the stoichiometry of the TCR/CD3 complex with one β and two ε-subunits could be confirmed, however, with a small uncertainty regarding the potential presence of β-subunit dimers.

In a general TOCCSL assay, accidental coincidence of protein clusters can lead to the false-positive detection of higher order oligomers and thus, to an overestimation of protein clusters with higher subunit count, a phenomenon that is more pronounced at high protein surface densities. Additionally, diffraction of the laser at the aperture edges can result in incompletely photobleached protein clusters. Thus, when analyzing TOCCSL after-bleach images, only the innermost area of the photobleached region is selected, and only the signals within that area are used for further analysis. Recovered single molecules can additionally be tracked over consecutive frames to determine their diffusion coefficient as well as for distinguishing true-positive and false-positive higher order oligomers (see more details in Sect. 5).

3.4 Two-Color TOCCSL

The TOCCSL protocol can also be applied in two colors [46] using two spectrally different fluorophores and two lasers of different wavelength that match the excitation maxima of the two fluorophores. In comparison to the one-color implementation of TOCCSL, where oligomerization is determined by brightness analysis of recovered single-molecule signals, the two-color TOCCSL implementation allows for direct counting of protein subunits via co-localization and is used to quantify relative fractions of monomer and dimer populations. Due to the different emission wavelengths of the two spectrally distinct fluorophores, their signal can be separated by an image splitter into two detection channels on the same camera chip (see Fig. 5 for the principle and an example of two-color TOCCSL). After irreversibly photobleaching all fluorescent molecules within an aperture-defined region, fluorescently labeled protein clusters diffuse back into the field of view during a recovery time. The recovered molecules are then imaged in both color channels.

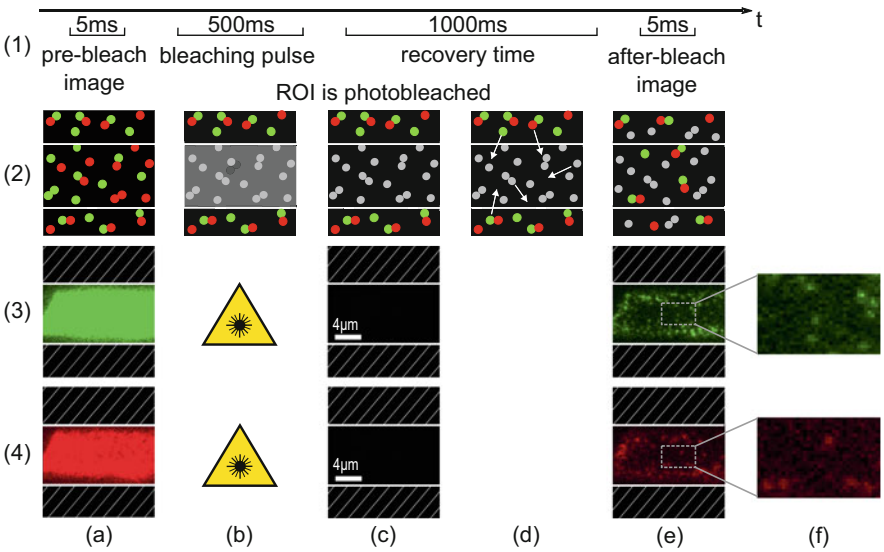

Fig. 5 A typical two-color TOCCSL imaging protocol. (1) Illumination timing Scheme. (2) Schematic illustration: (**a**) Control images are taken simultaneously in both color channels. (**b**), (**c**) The identical region of interest, defined by an aperture, is irreversibly photobleached in both color channels. (**d**) At the onset of the recovery process, fluorescent clusters carrying both spectrally distinct fluorescent molecules diffuse into the photobleached region. (**e**) The two spectrally different emission signals are imaged separately on the same camera chip. (**f**) Zoomed region from (**e**). (3) Example of a two-color TOCCSL experiment. CHO cells expressing GPI-anchored SNAP were labeled with Alexa Fluor 488 and Alexa Fluor 647 (green emission channel, i.e., Alexa Fluor 488 signals). (4) Two-color TOCCSL recordings of CHO SNAP-GPI cells labeled with Alexa Fluor 488 and Alexa Fluor 647 (red emission channel, i.e., Alexa Fluor 647 signals)

3.5 Co-localization Analysis

The two-color TOCCSL after-bleach images are used for co-localization analysis (see Fig. 6 for an example). To register both emission channels, a calibration is performed before each experiment. Multi-color beads, immobilized on a glass slide, are localized in the two spectrally separated detection channels. A correction matrix is determined, which specifies the necessary shift, stretch, and rotation of the second emission channel in respect to the first emission channel in order to register the position of the same bead imaged in both emission colors with accuracies of $<$20 nm.

For the co-localization analysis of two-color TOCCSL recordings, recovered single-molecule signals are localized in both detection channels and their positions are corrected using an affine transformation with the parameters determined by using the fluorescent beads. Signals found in both color channels are counted as co-localizations if their mutual distance is smaller than a predefined search-radius R. The algorithm can be tested by co-localizing single multi-color beads. The right choice of R depends on the inter-molecular distances of the observed protein

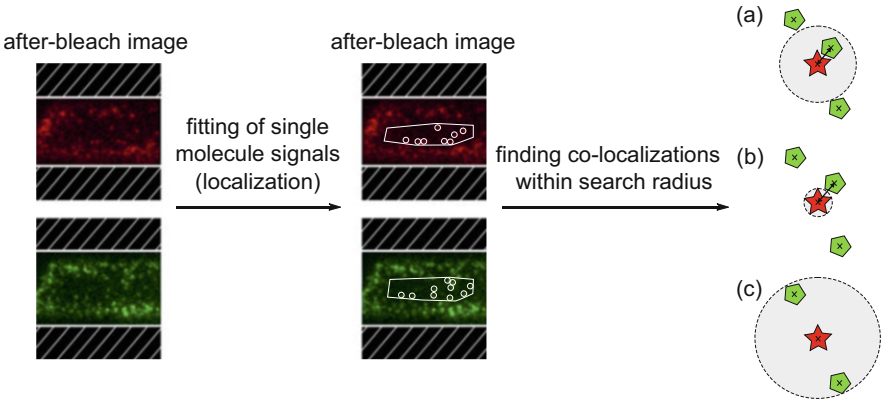

Fig. 6 After-bleach images are used for analysis: Recovered signals within selected analysis regions are localized, and the coordinates of both emission channels are corrected using multi-color fluorescent beads. (**a**) Pairs of two spectrally different fluorescence signals are counted as co-localizations if they are found within a predefined search-radius (dashed lines denote the borders of the search-region). (**b**) If the search-radius is chosen too small, dimer subunits do not co-localize and are falsely counted as monomers. (**c**) If the search-radius if chosen too large, true monomers co-localize and are counted as dimers (false-positive dimers). The rate of detected false-positive co-localizations strongly depends on the molecules density after recovery and increases towards the aperture edges. With the right choice of analysis region and recovery time, the number of false-positive dimers stays significantly below the number of true-positive dimers

complex, the emission wavelength of the fluorophore, the resolution of the microscopy setup, and the quality of fitting the positions. If R is chosen too small, protein dimers are not detected during co-localization analysis. In particular, if both color channels are not recorded simultaneously but rather temporally separated, diffusion of molecular complexes requires a larger search-radius. In contrast, if R is chosen too large, randomly encountered monomers co-localize and are detected as dimers, termed false-positive dimers (for more details, see Sect. 5).

To correct for false-positive dimers, coordinates of one color channel are mirrored alongside the x and y axis through the center of mass of all signals and the search algorithm for co-localizations is applied again, yielding the number of false-positive dimers. Dimer fractions are calculated considering all co-localized signals, subtracting all false-positive co-localized signals, and correcting for non-equimolar labeling as well as for unlabeled protein subunits. This correction is described in detail in [47]. Note, that in two-color TOCCSL experiments, only a fraction of true co-localized molecules can be detected directly, as depicted in Fig. 7.

The two-color implementation of TOCCSL was applied to exclude the presence of a minor fraction of TCRβ dimers. To this end, the β-subunit was labeled with a 1:1 mix of green and red fluorophores, and TCR oligomerization was quantified by co-localization analysis. For TCRβ, 0.4% of detected single-molecule events were visible in both color channels, i.e., were classified as true co-localized. In contrast,

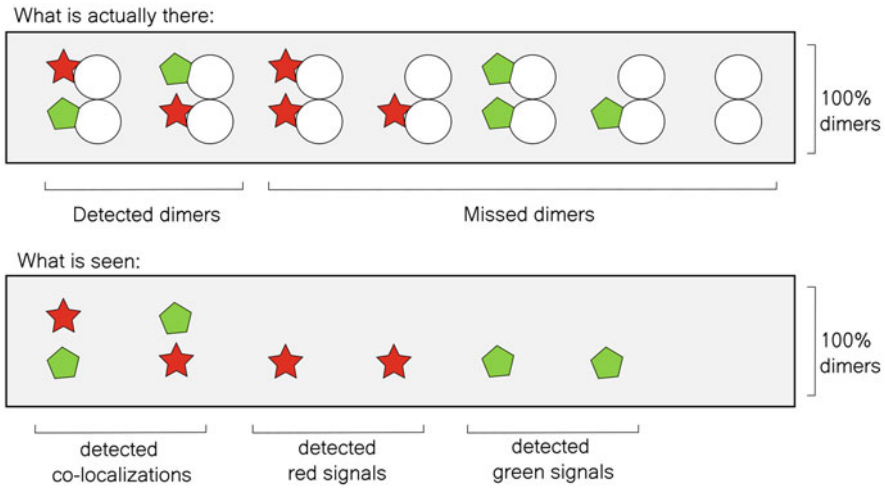

Fig. 7 Not all dimers are detected during co-localization analysis: Dimers carrying two spectrally identical fluorescent molecules as well as partially labeled dimers (labeling efficiency <1) are falsely counted as monomers as they appear only in one emission channel. Taking into account the number of detected co-localizations and the number of detected red and green emission signals, the dimer fraction determined from co-localization analysis can be corrected for non-equimolar labeling, for unlabeled protein subunits as well as for protein dimers carrying two identical fluorescent labels [47]

labeling of both of the ε-subunits or β-subunits via two different epitopes resulted in co-localization fractions two orders of magnitude higher [20].

The two-color TOCCSL assay can be combined with single-molecule FRET analysis for a more detailed characterization of molecular assemblies, e.g., by determination of their lateral extensions or inter-molecular distances. A combination with Single-Particle Tracking (SPT)/co-tracking of molecules in both emission channels achieves superior detection efficiencies, with the detection of only one co-localized trajectory out of hundred observations being statistically sufficient to rule out a false-positive observation [46].

4 Microscopy Setup

An exemplified microscopy system applicable for TOCCSL experiments is presented in Fig. 8.

The shown TOCCSL setup is based on a single-molecule fluorescence microscope with objective-based TIRF illumination. For precise and fast execution of the applied illumination timing protocol, directly modulated laser diodes are used in combination with a fast I/O module. Alternatively, the lasers can be modulated by acousto-optical modulators and mechanical shutters.

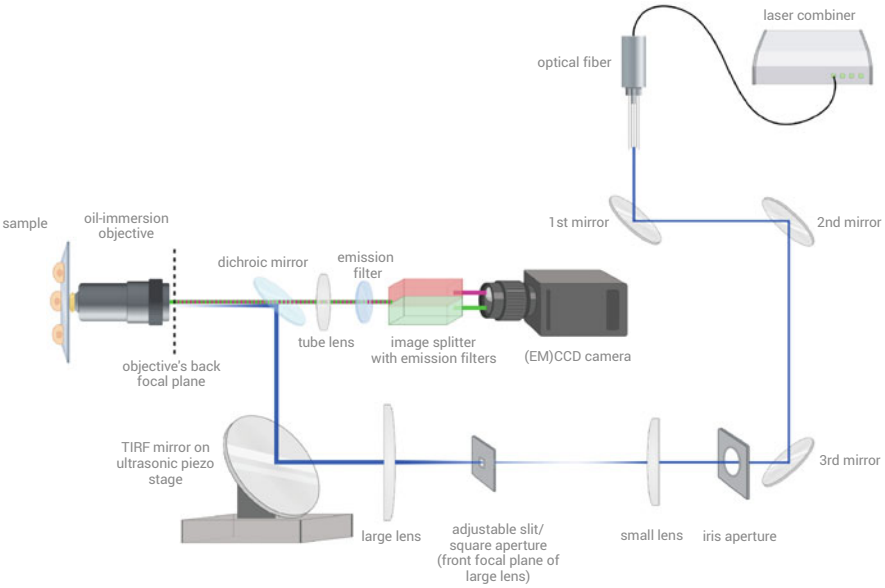

Fig. 8 Schematic illustration of a typical TOCCSL setup. Inside a multi-color laser combiner laser beams of differing wavelengths are overlaid with dichroic mirrors and coupled into an optical output fiber. The laser beams pass three mirrors and an iris aperture which is used to center the back-reflections originating from all following optical elements and to overlay them with the initial incoming beam. The beam is expanded and focused into the back focal plane of a high-NA oil immersion objective by using a two-lens system after being coupled into the microscope via a periscope. An adjustable slit/square aperture is placed at the front focal plane of the second lens (large lens), to confine the illuminated area at the sample plane. A mirror mounted to a piezo table at the bottom of the periscope allows for fast switching between Non-TIR and TIR modes. Excitation and emission light pass the same high-NA objective, which enables TIR excitation. A dichroic mirror separates the excitation beam from the emitted light. The emission light is further filtered by an emission band-pass filter suited to the used fluorophore and featuring an optical density of >6 to block totally reflected laser light. The emission signal is focused onto an (EM)CCD or sCMOS camera via a tube lens. For multi-color imaging, light is separated into two detection channels by an image splitter that is equipped with an additional dichroic mirror and optionally, two more emission filters

To obtain homogeneous illumination at the sample plane, the laser beam is focused into the back focal plane of the objective by a two-lens system. To ensure that the laser is entering the two-lens system parallel to the optical axis of the first lens, it is first guided via three adjustment-mirrors. The focal distance of the two-lens system must be calculated taking into account simple geometric optics (see Fig. 9).

Starting with the thin lens equations $\frac{1}{f_1} = \frac{1}{x_{o1}} + \frac{1}{x_{i1}}$ and $\frac{1}{f_2} = \frac{1}{x_{o2}} + \frac{1}{x_{i2}}$ for both lenses, they can be rewritten as $x_{i1} = \frac{x_{o1} \cdot f_1}{x_{o1} - f_1}$ and $x_{i2} = \frac{x_{o2} \cdot f_2}{x_{o2} - f_2}$.

With $d = x_{i1} + x_{o2} \Rightarrow x_{o2} = d - x_{i1}$ and x_{i1} inserted from above the front focal length of the two-lens system is given by

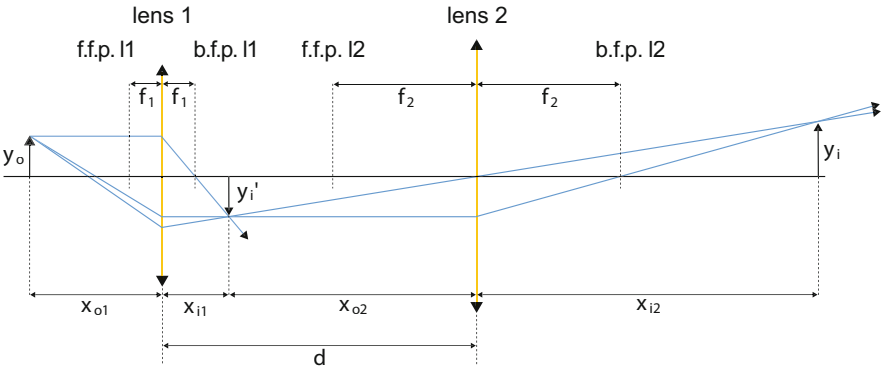

Fig. 9 Schematic illustration of a two-lens system. f.f.p. l1/2 and b.f.p. l1/2 denote the front focal plane and the back focal plane, respectively, and f_1/f_2 the focal length of the respective lens. The collimated (parallel) rays are focused at a distance x_{o1} + x_{i1} from the laser source, where an intermediate image of height y_i' is formed. Subsequently, the beam is focused once more at a distance x_{o2} + x_{i2} from the intermediate image, creating the final image of height y_i. x_{o1} and x_{o2} denote the distances from the object to the respective lens, x_{i1} and x_{i2} the distances from the respective lens to the image, and y_o the object height. The right choice of lenses and their respective distance d from each other ensures that the beam is focused into the back focal plane of the objective

$$x_{i2} = \frac{\left(d - \frac{x_{o1} \cdot f_1}{x_{o1} - f_1}\right) \cdot f_2}{d - \frac{x_{o1} \cdot f_1}{x_{o1} - f_1} - f_2} \tag{3}$$

Due to the collimated laser emitting a parallel beam, the object y_o can be considered to be infinitely far away and thus

$$f.f.l. = \lim_{x_{o1} \to \infty} x_{i2} = \frac{f_2 \cdot (d - f_1)}{d - (f_1 + f_2)} \tag{4}$$

The two lenses have to be chosen such, that the front focal length of the two-lens system is at the exact position of the objective's back focal plane. The laser is coupled into the microscope body via a periscope. Emission and excitation light both pass the same objective. To separate the excitation light from the Stokes-shifted emission light it, a dichroic mirror is used that reflects the excitation beam but transmits the spectrum of the emitted light. The emitted light is filtered from reflected excitation light and background by distinct emission filters.

For the implementation of TIRF, a mirror is used to shift the beam parallel to the optical axis. For this purpose, the mirror is mounted to a high-speed piezo table positioned behind the two-lens system, which allows for fast switching between TIR and non-TIR configuration (below 30 ms). Bleaching in non-TIR configuration and switching to TIR configuration when recording the recovery of single fluorescent molecules improves the signal-to-noise ratio, especially for cellular systems with high background signal due to intracellular fluorescence.

To restrict the excitation/illumination during imaging and photobleaching to a well-defined area of the cellular plasma membrane, a field stop, i.e., an adjustable slit/square aperture, is placed into the laser beam path at a sample-conjugated plane. Photobleaching of arbitrary shapes can be implemented by using a xy-laser scanning unit [48]. Images are recorded with an electron-multiplying charge-coupled device (EMCCD) or a scientific complementary metal-oxide-semiconductor (sCMOS) camera, that exhibit high read-out speed at low noise. For the two-color implementation of TOCCSL an image splitter is used to record the emitted fluorescence of the two spectrally different fluorophores on separate positions of the same camera chip.

5 Choice of Parameters

5.1 Choice of Recovery Time, Search-Radius and Analysis Region

The choice of t_{rec} depends on the mobility of the observed protein complexes, as well as its surface density and the size of the aperture. It should be chosen such, that multiple single-molecule signals per analysis region can be analyzed to obtain sufficient statistics [39]. However, the higher t_{rec}, the more molecules diffuse back into the field of view, which ultimately leads to an increase in surface density and thus to a higher fraction of false-positive co-localizations that contribute to the overestimation of higher order oligomers.

The fraction of false-positives scales with the co-localization search-radius as well as the protein surface density ρ. For a TOCCSL assay, assuming all protein clusters are randomly distributed over the surface, the probability for one of them to be located within a threshold distance R around another protein cluster is given by [46].

$$fp = 1 - \exp\left(-R^2 \cdot \pi \cdot \rho\right) \tag{5}$$

As the recovery proceeds from the aperture edges, the surface density after recovery increases in radial direction within the photobleached area. As *fp* depends on the surface density, it increases towards the aperture edges. Thus, molecules close to the aperture edges are excluded from the analysis. The higher t_{rec}, the more signals fill the photobleached spot, yielding an increase in *fp*. To keep *fp* at an approximately constant and low value, the area of the analysis region should be chosen smaller with increasing t_{rec}. The right choice of t_{rec} and an appropriate selection of the analysis area ensures that *fp* remains significantly below the number of detected true-positive dimers. For small fractions of true-positive dimers, this means that an extreme dilution of detected molecules and thus, the selection of a small analysis region is needed to ensure even smaller false-positive rates. This results in a reduced number of detectable events. Consequently, a high number of experiments is required.

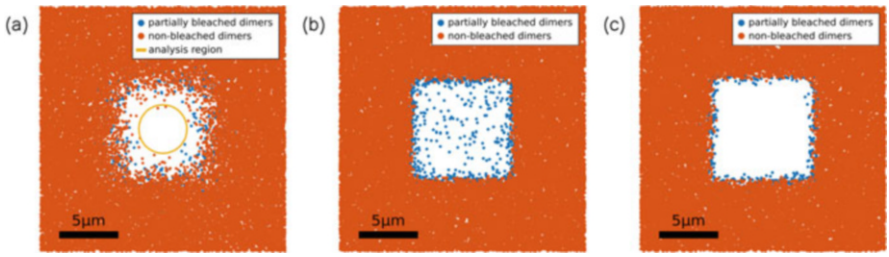

Fig. 10 Simulated after-bleach images for an initial protein surface density of $\rho = 100$ dimers/µm^2, a diffusion coefficient of $D = 0.5$ µm^2/s, a photobleaching intensity of $I = 5.32$ kW/cm^2 and each protein subunit carrying one GFP molecule (labeling efficiency = 1). (**a**) Simulation for a population of 100% dimers, $t_{\text{bleach}} = 400$ ms and $t_{\text{rec}} = 1$ s. The ideal choice of analysis region ensures that <20% false-positive dimers are detected. (**b**) If the chosen bleaching time is too short (e.g., $t_{\text{bleach}} = 100$ ms) partially bleached molecules remain within the photobleached region at $t_{\text{rec}} = 0$ s. (**c**) The edge zone of the aperture-defined region exhibits a high concentration of partially bleached dimers at $t_{\text{rec}} = 0$ s for a typical experimental bleaching time of 400 ms. Parts of this figure were taken from [49]

Figure 10a illustrated the right choice for the analysis region with <20% false-positive detections.

To further reduce *fp*, single-molecules can be tracked over consecutive images. Signals, that co-localize by coincidence move randomly and will separate over time, whereas true-positive oligomers exhibit a correlated movement and will remain associated (see also Sect. 3.5).

The surface density of protein clusters can be determined from the pre-bleach images of the TOCCSL sequence, by dividing the mean intensity per µm^2 by the corresponding single-molecule brightness obtained from the Gaussian fit. The protein surface densities in the after-bleach images can be determined by counting the number of analyzed diffraction-limited spots and dividing it by the area of the analysis region.

5.2 *Choice of Photobleaching Time*

Photobleaching is a stochastic process and depends on the illumination intensity at the sample plane as well as t_{bleach}. Due to diffraction at the aperture edges, the photobleaching probability is also a function of the molecules' coordinates within the photobleached area. The aperture-limited laser intensity profile, used in a TOCCSL experiment, typically exhibits an oscillating plateau bordered by an exponentially decreasing edge region, in which the photobleaching probability of fluorophores is reduced.

An appropriate choice of t_{bleach} and laser intensity is required, so that all fluorescently labeled molecules within the photobleached area of the sample are irreversibly switched off. The laser intensity and time needed for photobleaching strongly

depend on the imaged fluorophore and its photobleaching probability and must be determined experimentally. For this purpose, a control image is recorded immediately after photobleaching. If the control image exhibits detectable single-molecule signals or high fluorescent background, the photobleaching intensity and t_{bleach} have to be increased (see Fig. 10b for an example of t_{bleach} being too short and how it affects the detection of molecular dimers).

However, protein clusters diffuse in and out of the aperture-defined region during photobleaching. Additionally, they experience an overall reduced laser intensity and consequently, a decreased bleaching probability at the aperture edges. Thus, increasing the photobleaching intensity is advantageous over increasing t_{bleach}, as the extended illumination at the aperture edges increases the number of incompletely photobleached protein clusters, with one or more protein subunits remaining fluorescently labeled (see Fig. 10c for an example of partial bleaching at the edges of the aperture). On the other hand, the laser intensity during imaging should be kept low to further avoid partial photobleaching of protein clusters. The ideal laser intensity during imaging depends on the observed fluorophore as well as the signal-to-noise ratio after photobleaching. To further reduce fluorescent background, especially in live cell experiments, photobleaching in non-TIR configuration can be performed. The contrast of recovered single-molecule signals at the bottom of the cell membrane is always increased in TIR configuration.

5.3 Fluorescent Labels

As for all fluorescence microscopy experiments, the fluorescent label and the conjugation method need to be chosen with care. In the following, a few considerations are listed on how to find the optimum labeling strategy for TOCCSL experiments:

5.3.1 No Unspecific Binding/Detection of Fluorophores

Unspecific but stable binding of labels to the cover-glass does not affect the outcome of a TOCCSL experiment because of the photobleaching step during the execution of the TOCCSL protocol. Only the initial apparent surface density is increased by these immobile events. More important is to avoid unspecific interactions of organic dyes with the bilayer or glycocalyx of the plasma membrane. Here, fluorophores can diffuse back into the analyzed region and alter the result. As long as the fluorophores are highly hydrophilic, i.e., soluble in the medium used in the experiment, these membrane interactions can be neglected. Examples of organic dyes showing strong or nearly no preferences to interact with synthetic membranes can be found in [50].

Using fluorescent proteins (FPs) often causes unspecific detection events and an increased background due to a potential high abundance in the cytosol and inner membranes of the ER and the Golgi apparatus. Photobleaching in non-TIR

configuration efficiently decreases this background but cannot avoid the false-positive detection of FPs located in membrane-proximal vesicles. Single-particle tracking of recovered events allows to distinguish free diffusing molecules of interest from directed motion of vesicles via mean-square-displacement versus time-lag analysis [51].

5.3.2 Fast and Efficient Photobleaching While Keeping a Good Signal-to-Noise Ratio

The ideal fluorescent label for TOCCSL bleaches instantly upon high-power laser irradiation while concomitantly yielding a high number of photons in the after-bleach images recorded at low-power excitation. Practically, bleaching-stable dyes as well as fluorophores prone to blinking should be avoided. Most FPs compatible with single-molecule imaging, and non-blinking/non-bleaching-stable organic dyes are suited for one- or two-color TOCCSL applications. Rather than the countless number of different dyes nowadays offered, the availability of appropriate high-power and directly modulated laser sources is limited, rendering 488 nm or 640 nm laser diodes with ~200 mW output power optimal TOCCSL light sources.

5.3.3 Minimal-Invasive Conjugation to Biomolecule of Interest Possible

The type of fluorescent label determines the method used for conjugation to the biomolecule of interest. While FPs can be conjugated on a genetic level directly to proteins, organic dyes need to be conjugated via other molecules to label the target. In both cases, the conjugation must not affect the function of the biomolecule, e.g., the correct binding of ligands, enzymatic activity, or function of kinases. Another important aspect is the size of the fluorescent label, which should be as small as possible to avoid steric hindrance or size exclusion effects. While an antibody is about 180 kD in size, an antibody fragment (Fab) is only ~60 kD, and a single chain variable fragment (scFv) just about 28 kD (see Fig. 11 for a comparison of labels). The latter two are preferred, because they are monovalent binders. In contrast, an antibody is divalent and can lead to cross-linking of target molecules. Typical sizes of FPs or other genetic labels such as SNAP, CLIP, or Halo-tags (for a comparison of structure and kinetics, see [52]) are in the range of 20–30 kD. For the latter class, organic dyes with ~1 kD are enzymatically linked via the functional protein tags. Another category of small binders involves fluorescently labeled single domain nanobodies with a size of only ~15 kD. These binders are directed against FPs, as for the GFP-nanobody [53], or against peptides, as for the ALFA [54]- Spy [55]- or spot [56]-tag nanobody.

The close proximity of organic dyes to amphiphilic biomolecules also strongly influences their behavior; the influence can be minimized by, e.g., using neutral crosslinkers such as polyethylene glycol (PEG) [57].

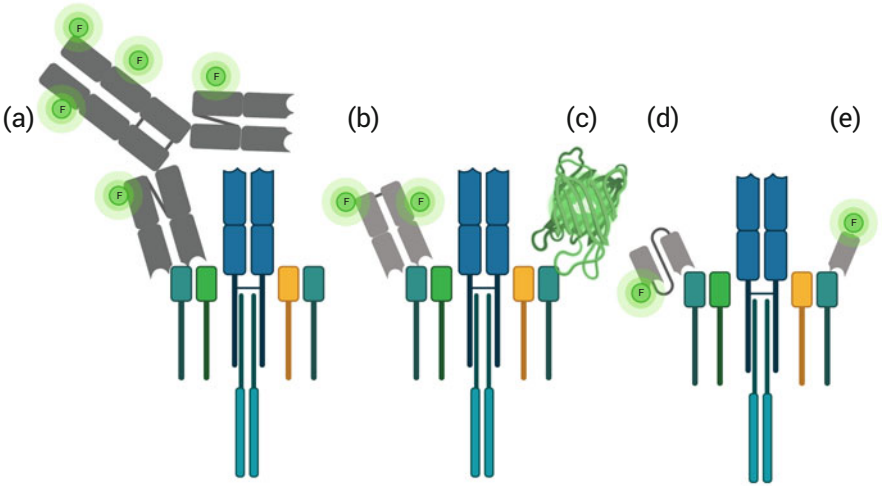

Fig. 11 Examples for labeling the TCR/CD3 complex. (**a**) Primary, NHS-labeled IgG antibody with a molecular weight (M_W) of ~150 kD, which features two epitope binding sites. (**b**) Via enzymatic digestion, Fabs with $M_W \sim 50$ kD can be generated and randomly labeled with NHS-functionalized organic dyes. (**c**) Genetically fused fluorescent proteins or tags (in the shown example GFP with a $M_W \sim 28$ kD) yield a 1:1 labeling stoichiometry, but can influence functionality, expression, and targeting of the protein complex. (**d**) Engineered and site-specifically labeled scFv represents a small ($M_W \sim 27$ kD), stoichiometric binder. (**e**) Nanobodies, only half the size of an scFv ($M_W \sim 15$ kD), are one of the smallest probes, which can be functionalized with exactly one fluorophore. For TOCCSL, small, monomeric, and site-specifically labeled probes (**c**–**e**) are preferred. Created with BioRender.com

In addition, also the conjugation of organic dyes to binder molecules like Fabs needs to be minimal invasive: if Fabs carry more than two organic dyes linked via NHS-labeling, the binding kinetics are strongly affected and in most cases only Fabs with no or just one dye are able to bind the protein of interest with high affinity [58].

5.3.4 Labeling Stoichiometry

Ideally, every molecule of interest carries exactly one fluorophore to allow straightforward brightness-based analysis of one-color TOCCSL experiments. This is less important for co-localization-based two-color TOCCSL experiments if the brightness in individual color channels is not considered. Genetically attaching a (monomeric)FP or protein/peptide tag to the biomolecule of interest causes in most cases a 1:1 labeling stoichiometry of biomolecule:FP/organic dye. However, for all protein tags, the maturation efficiency needs to be considered. Slow folding of proteins would deprive them from detection. In addition, labeling efficiency plays an important role for tags, where functionalized dyes need to be enzymatically linked.

1:1 labeling stoichiometries are also achieved by using nanobodies or scFvs. Via free cysteines, maleimide-functionalized dyes can be site-specifically attached. In

principle, also Fabs labeled non-specifically at primary amines via succinimidylester-functionalized dyes can be used for brightness analysis. However, care must be taken when recording the monomer-brightness distribution. The distribution will include single- and double-labeled Fabs and will differ significantly from a distribution of a single dye. Using secondary antibody labeling or fluorescent primary antibodies should be avoided due to their multi- and divalent binding affinity, respectively. In addition, quenching is observed for many dyes, if more than two dyes are present per antibody.

For determining the stoichiometry of the TCR/CD3 complex, the organic dye molecules Alexa Fluor 488 and Alexa Fluor 647 conjugated to an scFv against the ε- or β-subunit were chosen as the best fitting label for the following reasons:

1. Both organic dyes are hydrophilic and show a very low preference for interacting with membranes [50].
2. Alexa Fluor 488/647 is bright and easy to bleach due to its high/medium quantum yield and medium/high extinction coefficient.
3. The combination of dyes allows for efficient detection of (single-molecule) FRET (Förster radius $R_0 = 5.6$ nm).
4. scFv can be site-specifically and efficiently conjugated with exactly one fluorophore (protein-to-dye ratio ranged between 0.95 and 1.0 [20]).
5. The chosen scFvs bind efficient and strong (half-life time is 44 min [20]) and are only 1/6 of the size of a regular antibody.

6 TOCCSL Applications

One- and two-color TOCCSL applications have been used to address the stoichiometry of various plasma membrane proteins. In the following, a tabular and chronologically overview of TOCCSL applications is provided, which should serve as a guide to select certain parameters and labeling strategies and represent a source for finding further literature on TOCCSL (Tables 1 and 2).

Table 1 One-color TOCCSL applications

Protein/system	Labeling	Study/finding	Source
Anti-DNP antibody anchored to a supported lipid bilayer via DNP-DPPE	FITC via NHS-labeling, on average 4.5 FITC/antibody	TOCCSL proof-of-principle; labeling stoichiometry is conserved in TOCCSL	[40]
Lck-CFP-YFP on T24 cells	Yellow fluorescent protein (YFP)	Lck moves as small associates (monomer, dimers, and higher order multimers) in the membrane	[59]
GPI-anchored GFP (mGFP-GPI) on CHO cells Bodipy(FL)-GM1 on Jurkat T cells	Monomeric enhanced green fluorescent protein (mGFP), BodipyFL	mGFP-GPI forms cholesterol-dependent homo-dimers, Bodipy-GM1 clusters are present on Jurkat T cells	[43]
Bodipy-GM1 in a supported lipid bilayer and clustered by cholera toxinB (CTX-B)	BodipyFL	On average 1.4 Bodipy-GM1 molecules are bound per CTX-B	[46]
pMHC II (IEk/MCC(C))-Cy5 anchored to a supported lipid bilayer	Cy5 via maleimide chemistry	pMHC class II is monomeric at densities up to 500 molecules per μm^2	[60]
Orai1-mGFP	mGFP	Orai1 diffuses as homo-tetramer in the plasma membrane of T24 cells	[44]
Human serotonin transporter (hSERT)-mGFP on the plasma membrane of CHO cells	mGFP and fluorescent inhibitor JHC 1–64	Surface density independent and stable oligomerization of hSERT	[61]
mGFP-GPI on the plasma membrane of CHO cells	mGFP-GPI	mGFP-GPI homo-association is released by addition of oxidized phospholipids	[62]
Human serotonin transporter (hSERT)-mGFP in the ER & plasma membrane of CHO cells	mGFP	SERT oligomerization at the plasma membrane depends on PIP2 levels; SERT subunits rearrange in the ER	[63]
CD3ε and CD3β on murine primary T cells adhered to supported lipid bilayers	scFv-Alexa Fluor 647 coupled via maleimide chemistry	The TCR/CD3 complex consists of one CD3β and two CD3ε subunits; there exists no higher TCR oligomers on the membrane of resting T cells	[20]
Human dopamine transporter (hDAT) in the plasma membrane of CHO cells	mGFP	Monomers and dimers of hDAT coexist, no higher oligomers; dimers are stable over several minutes	[64]
mGFP-GPI on the plasma membrane of CHO cells	mGFP	Antimicrobial peptides influence the homo-association of mGFP-GPI	[65]

Table 2 Two-color TOCCSL applications

Protein/system	Labeling	Study/finding	Source
Bodipy-GM1 in a supported lipid bilayer and clustered by cholera toxin B (CTX-B)	BodipyFL-GM1 and CTX-B-Alexa Fluor 647	On average 1.4 Bodipy-GM1 molecules are bound per CTX-B	[46]
CD3ε and CD3β on murine primary T cells adhered to supported lipid bilayers	scFv-Alexa Fluor 488 and 647 coupled via maleimide chemistry	The TCR/CD3 complex consists of one CD3β and two CD3ε subunits; there exists no higher TCR oligomers on the membrane of resting T cells	[20]
ErbB2 and ErbB3 in CHO cells	Fab-Alexa Fluor 488 and 647 linked via NHS-ester	ErbB3 is activated via homo-dimerization and hetero-dimerization with ErbB2	[47]

References

1. Clevers H, Alarcon B, Wileman T, Terhorst C (1988) The T cell receptor/CD3 complex: a dynamic protein ensemble. Annu Rev Immunol 6:629–662
2. Dong D et al (2019) Structural basis of assembly of the human T cell receptor–CD3 complex. Nature 573:546–552
3. Ottschytsch N, Raes A, Van Hoorick D, Snyders DJ (2002) Obligatory heterotetramerization of three previously uncharacterized Kv channel α-subunits identified in the human genome. Proc Natl Acad Sci U S A 99:7986–7991
4. Yellen G (2002) The voltage-gated K+ channels and their relatives. Nature 419:35–42
5. Milligan G (2004) G protein-coupled receptor dimerization: function and ligand pharmacology. Mol Pharmacol 66:1–7
6. Lemmon MA, Schlessinger J (2010) Cell signaling by receptor tyrosine kinases. Cell 141: 1117–1134
7. Kusumi A, Tsunoyama TA, Hirosawa KM, Kasai RS, Fujiwara TK (2014) Tracking single molecules at work in living cells. Nat Chem Biol 10:524–532
8. Suzuki KGN et al (2012) Transient GPI-anchored protein homodimers are units for raft organization and function. Nat Chem Biol 8:774–783
9. Yáñez-Mó M, Barreiro O, Gordon-Alonso M, Sala-Valdés M, Sánchez-Madrid F (2009) Tetraspanin-enriched microdomains: a functional unit in cell plasma membranes. Trends Cell Biol 19:434–446
10. Simons K, Ikonen E (1997) Functional rafts in cell membranes. Nature 387:569–572
11. Douglass AD, Vale RD (2005) Single-molecule microscopy reveals plasma membrane microdomains created by protein-protein networks that exclude or trap signaling molecules in T cells. Cell 121:937–950
12. Vrljic M, Nishimura SY, Brasselet S, Moerner WE, McConnell HM (2002) Translational diffusion of individual class II MHC membrane proteins in cells. Biophys J 83:2681–2692
13. Manley S et al (2008) High-density mapping of single-molecule trajectories with photoactivated localization microscopy. Nat Methods 5:155–157
14. Betzig E et al (2006) Imaging intracellular fluorescent proteins at nanometer resolution. Science 313:1642–1645
15. Hess ST, Girirajan TP, Mason MD (2006) Ultra-high resolution imaging by fluorescence photoactivation localization microscopy. Biophys J 91:4258–4272
16. Rust MJ, Bates M, Zhuang X (2006) Sub-diffraction-limit imaging by stochastic optical reconstruction microscopy (STORM). Nat Methods 3:793–795
17. Heilemann M et al (2008) Subdiffraction-resolution fluorescence imaging with conventional fluorescent probes. Angew Chem Int Ed Engl 47:6172–6176

18. Pertsinidis A, Zhang Y, Chu S (2010) Subnanometre single-molecule localization, registration and distance measurements. Nature 466:647–651
19. Lelek M et al (2021) Single-molecule localization microscopy. Nat Rev Methods Prim 1:39
20. Brameshuber M et al (2018) Monomeric TCRs drive T cell antigen recognition. Nat Immunol 19:487–496
21. Rossboth B et al (2018) TCRs are randomly distributed on the plasma membrane of resting antigen-experienced T cells. Nat Immunol 19:821–827
22. Baumgart F et al (2019) What we talk about when we talk about nanoclusters. Methods Appl Fluoresc 7:13001
23. Platzer R et al (2020) Unscrambling fluorophore blinking for comprehensive cluster detection via photoactivated localization microscopy. Nat Commun 11:4993
24. Tanaka KAKK et al (2010) Membrane molecules mobile even after chemical fixation. Nat Methods 7:865–866
25. Hoffman DP et al (2020) Correlative three-dimensional super-resolution and block-face electron microscopy of whole vitreously frozen cells. Science 367(6475):eaaz5357
26. Weisenburger S et al (2014) Cryogenic colocalization microscopy for nanometer-distance measurements. ChemPhysChem 15:763–770
27. Kaufmann R et al (2014) Super-resolution microscopy using standard fluorescent proteins in intact cells under cryo-conditions. Nano Lett 14:4171–4175
28. Hell SW, Wichmann J (1994) Breaking the diffraction resolution limit by stimulated emission: stimulated-emission-depletion fluorescence microscopy. Opt Lett 19:780–782
29. Klar TA, Jakobs S, Dyba M, Egner A, Hell SW (2000) Fluorescence microscopy with diffraction resolution barrier broken by stimulated emission. Proc Natl Acad Sci U S A 97: 8206–8210
30. Hell SW (2007) Far-field optical nanoscopy. Science 316:1153–1158
31. Sahl SJ, Hell SW, Jakobs S (2017) Fluorescence nanoscopy in cell biology. Nat Rev Mol Cell Biol 18:685–701
32. Blom H, Widengren J (2017) Stimulated emission depletion microscopy. Chem Rev 117:7377–7427
33. Kimble HJ, Dagenais M, Mandel L (1977) Photon antibunching in resonance fluorescence. Phys Rev Lett 39:691–695
34. Sýkora J et al (2007) Exploring fluorescence antibunching in solution to determine the stoichiometry of molecular complexes. Anal Chem 79:4040–4049
35. Ta H, Kiel A, Wahl M, Herten DP (2010) Experimental approach to extend the range for counting fluorescent molecules based on photon-antibunching. Phys Chem Chem Phys 12: 10295–10300
36. Ta H et al (2015) Mapping molecules in scanning far-field fluorescence nanoscopy. Nat Commun 6:7977
37. Balzarotti F et al (2017) With minimal photon fluxes. Science 355:606–612
38. Schmidt R et al (2021) MINFLUX nanometer-scale 3D imaging and microsecond-range tracking on a common fluorescence microscope. Nat Commun 12:1478. https://doi.org/10.1038/s41467-021-21652-z
39. Brameshuber M, Schutz GJ (2012) Detection and quantification of biomolecular association in living cells using single-molecule microscopy. Methods Enzym 505:159–186
40. Moertelmaier M, Brameshuber M, Linimeier M, Schütz GJ, Stockinger H (2005) Thinning out clusters while conserving stoichiometry of labeling. Appl Phys Lett 87:1–3
41. Edidin M, Zagyansky Y, Lardner TJ (1976) Measurement of membrane protein lateral diffusion in single cells. Science 191:466–468
42. Axelrod D, Koppel DE, Schlessinger J, Elson E, Webb WW (1976) Mobility measurement by analysis of fluorescence photobleaching recovery kinetics. Biophys J 16:1055–1069
43. Brameshuber M et al (2010) Imaging of mobile long-lived nanoplatforms in the live cell plasma membrane. J Biol Chem 285:41765–41771

44. Madl J et al (2010) Resting state Orai1 diffuses as homotetramer in the plasma membrane of live mammalian cells. J Biol Chem 285:41135–41142
45. Mutch SA et al (2007) Deconvolving single-molecule intensity distributions for quantitative microscopy measurements. Biophys J 92:2926–2943
46. Ruprecht V, Brameshuber M, Schütz GJ (2010) Two-color single molecule tracking combined with photobleaching for the detection of rare molecular interactions in fluid biomembranes. Soft Matter 6:568–581
47. Váradi T et al (2019) Homo- and heteroassociations drive activation of ErbB3. Biophys J 117: 1935–1947
48. Belyy V et al (2017) PhotoGate microscopy to track single molecules in crowded environments. Nat Commun 8:13978
49. Kiesenhofer D (2017) Development of Monte Carlo simulations for characterization and optimization of TOCCSL experiments. TU Wien
50. Hughes LD, Rawle RJ, Boxer SG (2014) Choose your label wisely: water-soluble fluorophores often interact with lipid bilayers. PLoS One 9:e87649
51. Wieser S, Schutz GJ (2008) Tracking single molecules in the live cell plasma membrane-Do's and Don't's. Methods 46:131–140
52. Wilhelm J et al (2021) Kinetic and structural characterization of the self-labeling protein tags HaloTag7, SNAP-tag, and CLIP-tag. Biochemistry 60:2560–2575
53. Rothbauer U et al (2006) Targeting and tracing antigens in live cells with fluorescent nanobodies. Nat Methods 3:887–889
54. Götzke H et al (2019) The ALFA-tag is a highly versatile tool for nanobody-based bioscience applications. Nat Commun 10:1–12
55. Khairil Anuar INA et al (2019) Spy&Go purification of SpyTag-proteins using pseudo-SpyCatcher to access an oligomerization toolbox. Nat Commun 10:1–13
56. Virant D et al (2018) A peptide tag-specific nanobody enables high-quality labeling for dSTORM imaging. Nat Commun 9:1–14
57. Honigmann A et al (2014) Scanning STED-FcS reveals spatiotemporal heterogeneity of lipid interaction in the plasma membrane of living cells. Nat Commun 5:5412
58. Szabo A et al (2018) The effect of fluorophore conjugation on antibody affinity and the photophysical properties of dyes. Biophys J 114:688–700
59. Schwarzenbacher M et al (2008) Micropatterning for quantitative analysis of protein-protein interactions in living cells. Nat Methods 5:1053–1060
60. Huppa JB et al (2010) TCR-peptide-MHC interactions in situ show accelerated kinetics and increased affinity. Nature 463:963–967
61. Anderluh A et al (2014) Single molecule analysis reveals coexistence of stable serotonin transporter monomers and oligomers in the live cell plasma membrane. J Biol Chem 289: 4387–4394
62. Brameshuber M et al (2016) Oxidized phospholipids inhibit the formation of cholesterol-dependent plasma membrane nanoplatforms. Biophys J 110:205–213
63. Anderluh A et al (2017) Direct PIP 2 binding mediates stable oligomer formation of the serotonin transporter. Nat Commun 8:14089
64. Das AK et al (2019) Dopamine transporter forms stable dimers in the live cell plasma membrane in a phosphatidylinositol 4,5-bisphosphate independent manner. J Biol Chem 294:5632–5642
65. Schromm AB et al (2021) Cathelicidin and PMB neutralize endotoxins by multifactorial mechanisms including LPS interaction and targeting of host cell membranes. Proc Natl Acad Sci 118:e2101721118